Yagi-Uda nanoantenna enhanced metal-semiconductor-metal photodetector

W. Rieger,[1,2] J. J. Heremans,[1,a] H. Ruan,[2,3] Y. Kang,[2] and R. Claus[2]

[1]*Department of Physics, Virginia Tech, Blacksburg, Virginia 24060, USA*
[2]*NanoSonic, Inc., 158 Wheatland Dr., Pembroke, Virginia 24136, USA*
[3]*Department of Mechanical Engineering, Virginia Tech, Blacksburg, Virginia 24060, USA*

An array of 400 nanolithographic Yagi-Uda antennas on a metal-semiconductor-metal rectifier photodetector demonstrates control of wavelength selectivity and directivity. The nanoantenna array response is obtained using a direct electrical measurement approach. Resonances in rectified photocurrent are detected at the incident electromagnetic radiation of free-space wavelengths 1110 nm and 1690 nm, corresponding to scaled effective wavelengths of 388 nm and 776 nm, respectively. The scaling is consistent with a theory based on plasmonic effects in nanoscale devices at optical frequencies, and the two resonant wavelength modes are found to match at, respectively, full-wavelength and half-wavelength operation of the detector dipole element. Quantum efficiencies are estimated as 5.1% and 3.1% at 1110 nm and 1690 nm wavelengths, respectively, representing a fourfold increase over a device lacking the antenna array. *Published by AIP Publishing.* https://doi.org/10.1063/1.5038339

Nanoantennas operating at optical electromagnetic wavelengths and produced on solid-state substrates using nanofabrication techniques have formed a topic of interest since nanofabrication techniques have enabled their creation. A compelling feature of such nanoantennas lies in the promise to draw from the existing knowledge of RF antennas to design optical devices with functionalities that are difficult to obtain from materials properties alone. Nanoantennas have been studied in the context of focusing electric fields in scanning tunneling microscopy,[1] controlling optical transmission and reflection through optically designed surfaces,[1–4] studying non-linear optics,[5–7] and creating frequency selective photodetectors.[8–12] Yagi-Uda nanoantennas have been of particular interest[13–17] due to the Yagi-Uda geometry being well understood, and having excellent gain and directive properties. The Yagi-Uda geometry further lends itself well to nanofabrication.

Here, we report an electrical characterization of Yagi-Uda based nanoantenna arrays fabricated on a semiconductor surface where Schottky barriers are formed at the antenna-semiconductor interface. Such a structure is built into a metal-semiconductor-metal (MSM) electronically rectifying detector device to collect the photocurrent when the nanoantenna is photoexcited. The approach allows implementation of optically designed surfaces to practical photodetectors to achieve higher functionalities and efficiencies. Two aspects differentiating nanoantennas from macroscopic RF antennas underlie the present work. First, a loss of linearity in antenna scaling with wavelength occurs as wavelength and concomitant antenna element size are reduced. Plasmonic effects dominate at these length scales causing the loss in linearity and must be accounted for in design dimensions. Second, nanoantennas fabricated on substrates have a nonsingular feed point, arising from the impracticality of achieving the necessarily small electrical connections. Most nanoantenna studies to date, with exceptions,[8–12] have focused on optical measurement techniques, with interrogation occurring via optical transmission, reflection, and absorption. Although an effective means of determining resonant behavior, optical measurements limit real-world applicability. Since nanoantennas lack a singular feed point, concepts such as impedance and standing wave ratio, inherent to RF antenna design, now lack definite meaning. Instead, the whole system must be considered to recover equivalent concepts. Despite the differences, concepts of macroscopic RF antennas retain their usefulness to characterize solid-state nanoantennas and a basis for the present work is formed by a theoretical link derived between RF antennas and nanoantennas using the concept of effective wavelengths.

The nanoantenna characterization method used in this work consists of a direct electrical measurement of the rectified photocurrent generated by the nanoantennas, representing a step beyond nanoantenna work relying on optical characterization. While a rectified photocurrent measurement using an indium tin oxide (ITO) film and a back electrode has appeared,[8–12] the present work employs a measurement scheme omitting the ITO layer and directly measuring the photocurrent injected into the Si by the electric field concentrations at the nanoantenna elements. A MSM Schottky junction photodiode is formed, where the nanoantenna elements form one metal electrode, the Si forms the semiconductor, and two macroscopic Au counter contacts deposited on the Si form two other metal electrodes between which a voltage bias is applied. Photocurrent is measured across the resulting MSM diode. Photocurrent rectification from optical frequencies to low frequencies for lock-in amplifier detection (17 Hz) is achieved by the two junctions in the MSM diode, one of which is forward biased and the other reverse biased. Figure 1(a) depicts a schematic of the photocurrent measurements, and Figs. 1(b)–1(e) depicts aspects of the nanoantenna devices and measurements, as explained below. Generation of photocurrent is a multi-step process. This

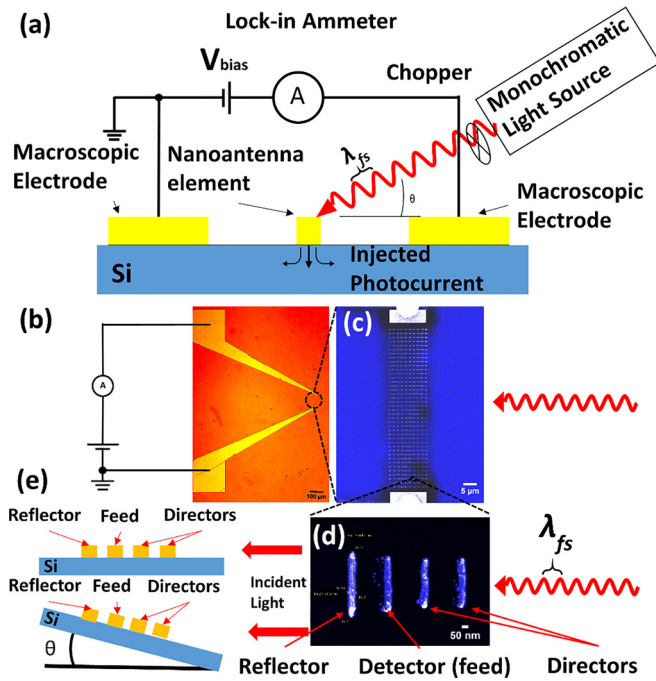a)Author to whom correspondence should be addressed: heremans@vt.edu

FIG. 1. (a) Schematic of the experimental setup and measurement scheme. Chopped monochromatic light is incident on the device at an angle, θ. (b) Enlarged view of the device highlighting the macroscopic electrodes. (c) SEM micrograph of the entire antenna array, with 400 Yagi-Uda nanoantennas occupying the space between the electrodes. (d) SEM micrograph of a single Yagi-Uda nanoantenna. Each nanoantenna is comprised of 4 elements with dimensions listed in Table I. (e) Side view of the measurement setup indicating angle, θ, of incident monochromatic light.

TABLE I. Design dimensions for the Yagi-Uda nanoantenna elements given $\lambda_{eff} = 776$ nm. Elements have a measured width of 58 nm. Elements have a height of 60 nm (10 nm Cr/50 nm Au). The uncertainty in the measured length across the array is ±5 nm.

Element	Design dimensions	Designed lengths (nm)	Measured lengths (nm)
Reflector	$\lambda_{eff}/1.75$	443	464
Detector	$\lambda_{eff}/2$	388	406
Directors	$\lambda_{eff}/2.25$	345	357
Element spacing	$\lambda_{eff}/3$	258	264

light wavelength λ_{fs} in the IR region of the spectrum, namely, $\lambda_{fs} \sim 1500$ nm. The effective incident wavelength λ_{eff} experienced by the nanoantennas differs from λ_{fs}, as detailed below.[19] Investigating the relation between λ_{eff} and λ_{fs} for Yagi-Uda geometries forms one of the aims of this work. A preliminary estimate of λ_{eff} given $\lambda_{fs} \approx 1500$ nm yields $\lambda_{eff} \approx 776$ nm, and hence $\lambda_{eff} = 776$ nm formed the starting point of the design in Table I. The designed lengths in Table I denote the nominal lithographic dimensions whereas measured lengths were evaluated from SEM micrographs.

The measurement setup consists of a broadband light source, an optical chopper operating at 17 Hz, a monochromator, a 3-axis translation and single-axis rotation sample stage, and a lock-in ammeter. The power density of the incident light is ~ 0.25 W/m^2. Translation adjustments are used to center the device [Figs. 1(a)–1(e)] in the illuminated spot at a constant distance of 10 cm from the monochromator aperture. The rotation axis allows the angle of incidence, θ, of the incident light to vary from the glancing ($\theta \approx 0°$) to normal angle ($\theta = 90°$) to the device plane [Figs. 1(d) and 1(e)]. The sample stage is enclosed in a metal enclosure shielding the photocurrent measurement from ambient light and stray electric fields. The device was biased at 1.0 V DC and the chopped photocurrent was measured by the lock-in amplifier. The incident λ_{fs} was varied from 1000 nm to 2000 nm. Measurements were obtained on both the nanoarray sample and blank sample, each at glancing angle ($\theta \approx 0°$) and at $\theta = 45°$.

Assuming a standard Yagi-Uda antenna directivity,[15–17] at $\theta \approx 0°$ the incident light wave vector is nearly aligned with the main lobe of the Yagi-Uda antenna receiving and transmitting directivity, while at $\theta = 45°$, the incident light wave vector alignment is not expected to coincide with the main lobe or side lobes. Half angular widths of Yagi-Uda antennas are found to be less than $32.5°$.[16] Measurements of photocurrent vs λ_{fs} are depicted in Figs. 2(a) and 2(b) for $\theta \approx 0°$ and $\theta = 45°$, respectively, for the nanoantenna sample and blank reference sample. Figure 2(a) indicates two resonances for $\theta \approx 0°$, for which photocurrent reaches a maximum in the nanoantenna sample, namely, at $\lambda_{fs} = 1110$ nm and at $\lambda_{fs} = 1690$ nm. As a reference, the photocurrent measurement in the blank sample for $\theta \approx 0°$ does not show resonances [Fig. 2(a)]. Likewise, in contrast to the measurement at $\theta \approx 0°$, data for $\theta = 45°$ does not indicate clear resonances [Fig. 2(b)]. A higher average photocurrent is measured for $\theta = 45°$ indicating that more hot electrons are generated with the $45°$ illumination. The comparison between data for $\theta \approx 0°$ and data for $\theta = 45°$ is consistent with the expected

process begins when the nanoantenna is illuminated with an appropriate wavelength to excite plasmons in the antenna devices. These plasmons can decay along multiple pathways.[18] The possible pathways include transfer of energy to phonons, reradiation, and injection of a hot electron into the metallic structure. If the injected hot electron is sufficiently energetic, it can overcome the Schottky barrier and move to the conduction band of the semiconductor [Fig. 1(a)].

The nanoantennas were fabricated on an n-Si (100) wafer, from which SiO$_2$ was removed by a buffered oxide etch. Photolithography, deposition of 10 nm Cr and 50 nm Au, and lift-off then created macroscopic electrodes with fingers extending towards the device area [Fig. 1(b)]. These macroscopic electrodes allow electrical connections to the measurement setup [Figs. 1(a) and 1(b)]. Subsequent electron-beam lithography, deposition of 10 nm Cr and 50 nm Au, and lift-off then created an array of 400 individual Yagi-Uda nanoantennas as well as rectangular electrodes flanking the array and overlapping the photolithographic electrodes [Fig. 1(c)]. As reference, a "blank" device was also produced, lacking only the array of nanoantennas. The dimensions of the nanoantenna elements on the active device are listed in Table I, and Fig. 1(d) depicts an individual nanoantenna. Each nanoantenna consists of nanorod elements assuming the roles of directors, reflector, and feed elements, equivalents to the elements of macroscopic Yagi-Uda antennas. In this work, we will refer to the feed element as the detector element, as the nanoantennas are operated in the receiving rather than the transmitting mode. The nanoantennas were initially designed to detect a free-space incident
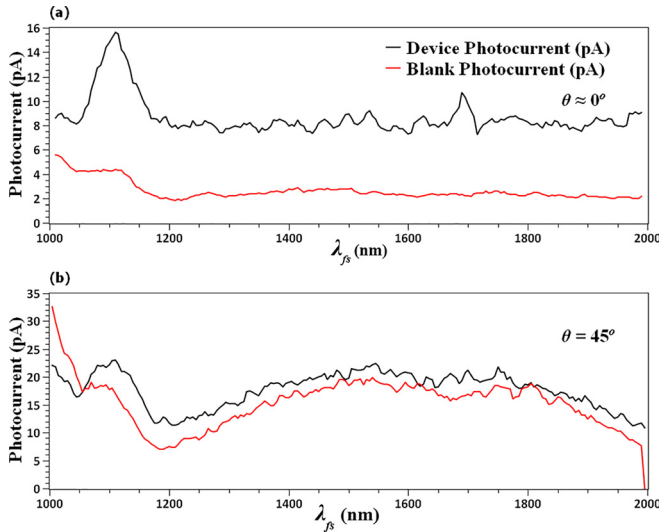
FIG. 2. (a) Photocurrent data *vs* λ_{fs}, for $\theta \approx 0°$. The black line represents the measured photocurrent on the nanoantenna device and the red line on the blank device. The nanoantenna device shows maxima at 1110 nm and 1690 nm corresponding to Yagi-Uda nanoantenna resonances. The blank device does not show resonances. (b) Photocurrent data *vs* λ_{fs}, for $\theta = 45°$. The black line represents the measured photocurrent on the nanoantenna device and the red line on the blank device. Consistent with the directivity of a Yagi-Uda antenna, no discernable maxima appear on a background showing broad features.

directivity of the Yagi-Uda nanoantennas, and the values where resonances are detected are consistent with the scaling properties of nanoantennas, as explained below.

The responsivities of the nanoantenna sample at $\theta \approx 0°$ are estimated at 46 mA/W at $\lambda_{fs} = 1110$ nm and at 31 mA/W at $\lambda_{fs} = 1690$ nm. The resulting quantum efficiencies are estimated at 5.1% and 3.1%, respectively. The responsivities of the blank sample are estimated at 11 mA/W at $\lambda_{fs} = 1110$ nm and at 5.7 mA/W at $\lambda_{fs} = 1690$ nm, yielding estimated quantum efficiencies of 1.2% and 0.64%, respectively. The nanoantenna sample thus shows quantum efficiencies increased fourfold over the blank sample. To improve the quantum efficiencies over this prototype nanoantenna sample, several avenues towards optimization are available, e.g., using the spatial distribution of the response. The array in the present work causes each nanoantenna to cast a shadow on the nanoantennas behind it. Thus, the nanoantennas on the array's leading edge contribute more to the photocurrent. Additionally, the band bending does not fall uniformly over the biased MSM device's cross-section. Further, the nanoantennas nearest the forward biased electrode are expected to contribute more to the photocurrent because the hot electrons are more likely to reach this electrode before experiencing energy loss.[20] The three mentioned effects will give rise to a spatial dependence of the response. The effects can be used towards an optimization of quantum efficiency, by using a lattice other than square to reduce shadowing, by changing the aspect ratio of the array to locate a larger number of nanoantennas closer to the electrodes and within regions of higher band bending, and by increasing the bias voltage[21] such that the hot electrons generated closer to the reverse biased electrode are more likely to reach the forward biased electrode. Additionally, Yagi-Uda antennas show a dependence on polarization, and higher efficiencies will result from a polarized light source at

the correct orientation. Since RF Yagi-Uda antennas are very efficient and MSM structures can show high quantum efficiencies,[21] future optimized devices can reach higher quantum efficiencies, while retaining the observed selectivity and directivity.

A useful aspect of RF antenna designs is a linear scaling of antenna geometry with the free-space wavelength, inherent in free-space electromagnetism. This linear scaling fails due to materials properties for λ_{fs} below the millimeter wave region. At these shorter wavelengths, the electric fields in the antenna elements assume a complicated pattern and are described by oscillations of free electrons in or on the surface of the metal antenna structure. These surface plasmons are of particular interest to the study of nanoantennas because they are able to couple to free-space electromagnetic waves.[22,23] The coupling of surface plasmons on a nanoantenna to incident light yields an effective wavelength, namely, the wavelength of free-space electromagnetic radiation that couples to the resonant plasmon oscillation. Theoretically, a scaling exists for these antennas, and a specific relation has been derived for antennas consisting of rod-like elements with a diameter much less than the wavelength of interest.[19] The scaling is derived by forcing a surface plasmon on a rod-like element. The element is considered as a cylindrical wave guide with boundary conditions for TM mode oscillations. Requiring the existence of these modes yields a relation between the free-space incident λ_{fs} and an effective incident wavelength λ_{eff} experienced by the nanoantenna.[19] As an approximation for the present Yagi-Uda nanoantennas, the following relation between λ_{fs} and λ_{eff} is used:[19]

$$\lambda_{eff} = \frac{\lambda_{fs}}{K} \sqrt{\frac{4\pi^2 K \left(R^2/\lambda_{fs}^2\right) z\left(\lambda_{fs}, K\right)}{1 + 4\pi^2 K \left(R^2/\lambda_{fs}^2\right) z\left(\lambda_{fs}, K\right)}} - \lambda_c. \quad (1)$$

In this expression, K indicates the relative permittivity of the dielectric (assumed uniform) in which the nanoantenna is embedded and λ_c indicates a capacitive contribution depending on the end radius R of the nanorod elements.[19] For perfect hemispherical nanorod ends, theory yields $\lambda_c = 4R$. Since the rod ends of the actual nanoantennas are likely not hemispherical and hence not characterized by fixed R, λ_c will be treated as an adjustable parameter to fit the measurements. Further, K is assumed real for a dielectric, and in the IR range of λ_{fs}, for Si $K \approx 3.5$ is estimated. Yet, the Au nanorods are deposited on Si ($K \approx 3.5$) and are exposed to ambient air ($K = 1$) at their free surfaces. Hence, K is also regarded as an adjustable parameter, with a physically acceptable range of values.

Figure 3 contains representative plots of λ_{eff} *vs* λ_{fs} (nearly straight lines) and indicates the influence of both K (effective dielectric medium) and λ_c (nanorod geometry), thereby highlighting their effect in understanding the measured incident λ_{fs} at resonance in terms of the calculated λ_{eff}. We note that in the relation of λ_{eff} *vs* λ_{fs}, varying K changes the slope and the intercept, while varying λ_c changes the intercept only. Figure 3 highlights the value $\lambda_{eff} = 776$ nm, of relevance if the length of the detector nanorod of each Yagi-Uda nanoantenna corresponds to approximately half λ_{eff}
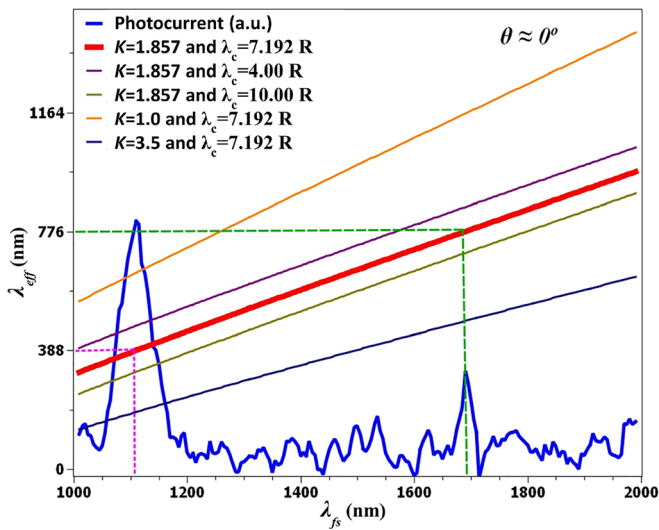
FIG. 3. Glancing angle ($\theta \approx 0°$) photocurrent data *vs* λ_{fs}, superimposed on λ_{eff} *vs* λ_{fs} as calculated from Eq. (1). For $K = 1.857$ and $\lambda_c = 7.192R$, Eq. (1) provides a best-fit correspondence between $\lambda_{eff} = 776$ nm and $\lambda_{eff} = 388$ nm and the two values of λ_{fs} where a photocurrent resonance is observed. For comparison, four other curves of λ_{eff} *vs* λ_{fs} calculated from Eq. (1) are shown, for various K and λ_c bracketing the best-fit values.

(half-wavelength resonant mode or first excited mode operation, the usual design operation for Yagi-Uda antennas), and highlights the value $\lambda_{eff} = 388$ nm, of relevance if the length of the detector nanorod corresponds to approximately a full λ_{eff} (full-wavelength resonant mode or second excited mode operation). In the fabricated nanoantennas, the rod ends are not perfect hemispheres and they possess a textured surface expected to increase the capacitance due to the nanorod ends, resulting in increased λ_c. Regarding K, an effective value $1.0 \leq K \leq 3.5$ is expected as an intermediate value for K between Si and air. As indicated in Fig. 3, Eq. (1) yields a best-fit correspondence (red line) between $\lambda_{eff} = 776$ nm and $\lambda_{eff} = 388$ nm and the two values of λ_{fs}, where a photocurrent resonance is observed (respectively, $\lambda_{fs} = 1110$ nm and $\lambda_{fs} = 1690$ nm) for $K = 1.857$ and $\lambda_c = 7.192R$. The best-fit value $\lambda_c > 4R$ is consistent with expectations and physically reasonable. The best-fit value $1.0 \leq K = 1.86 \leq 3.5$ is also consistent with the nanoantennas experiencing an effective dielectric medium intermediate between Si and air, as mentioned. Hence, Fig. 3 shows that the scaling between λ_{eff} *vs* λ_{fs} implied by Eq. (1) is consistent with the experimental results, when the dielectric environment and geometrical capacitive coupling effects are taken into account. The photocurrent measurements contained in Figs. 2(a) and 2(b) then also form a strong indication that the nanoantenna array shows the wavelength selectivity and the directivity expected from the Yagi-Uda geometry, and that nanoantennas can be used to impart these properties to a photodetector.

In conclusion, the present work advances the study of optical nanoantennas by using a fabrication process which integrates nanoantennas in a metal-Si-metal rectifier photodiode. The Yagi-Uda nanoantennas demonstrate wavelength selectivity and directivity. The wavelength selectivity follows a predictive scaling rule based on plasmonic effects, and is dependent on an effective discontinuous dielectric environment as well as on geometrical effects expressed via capacitive coupling to the environment. Future work can be directed at more refined photocurrent or signal extraction by optimized electron injection, at measuring the sensitivity to polarization of the nanoantennas, and at scaling to wider ranges of wavelengths in the IR and visible regions of the spectrum.

See supplementary material for current-voltage characteristics of the MSM structure and for information about the choice of the voltage bias point.

[1]P. Bharadwaj, B. Deutsch, and L. Novotny, Adv. Opt. Photonics **1**(3), 438–483 (2009).
[2]L. Novotny and N. van Hulst, Nat. Photonics **5**(2), 83–90 (2011).
[3]I. S. Maksymov, I. Staude, A. E. Miroshnichenko, and Y. S. Kivshar, Nanophotonics **1**(1), 65–81 (2012).
[4]X. Ni, N. K. Emani, A. V. Kildishev, A. Boltasseva, and V. M. Shalaev, Science **335**(6067), 427 (2012).
[5]X. Y. Xiong, L. J. Jiang, W. E. Sha, Y. H. Lo, and W. C. Chew, Sci. Rep. **6**, 18872 (2016).
[6]A. C. Lesina, P. Berini, and L. Ramunno, Opt. Mater. Express **7**(5), 1575–1580 (2017).
[7]B. Metzger, M. Hentschel, and H. Giessen, Nano Lett. **17**(3), 1931–1937 (2017).
[8]B. Y. Zheng, Y. Wang, P. Nordlander, and N. J. Halas, Adv. Mater. **26**(36), 6318–6323 (2014).
[9]A. Sobhani, M. W. Knight, Y. Wang, B. Zheng, N. S. King, L. V. Brown, Z. Fang, P. Nordlander, and N. J. Halas, Nat. Commun. **4**, 1643 (2013).
[10]S. Piltan and D. Sievenpiper, J. Appl. Phys. **122**(18), 183101 (2017).
[11]M. W. Knight, H. Sobhani, P. Nordlander, and N. J. Halas, Science **332**(6030), 702–704 (2011).
[12]M. W. Knight, L. Liu, Y. Wang, L. Brown, S. Mukherjee, N. S. King, H. O. Everitt, P. Nordlander, and N. J. Halas, Nano Lett. **12**(11), 6000–6004 (2012).
[13]A. G. Curto, G. Volpe, T. H. Taminiau, M. P. Kreuzer, R. Quidant, and N. F. van Hulst, Science **329**(5994), 930–933 (2010).
[14]T. Kosako, Y. Kadoya, and H. F. Hofmann, Nat. Photonics **4**(5), 312–315 (2010).
[15]L. Ma, J. Lin, Y. Ma, B. Liu, J. Tan, and P. Jin, Opt. Commun. **368**, 197–201 (2016).
[16]I. S. Maksymov, A. R. Davoyan, A. E. Miroshnichenko, C. Simovski, P. Belov, and Y. S. Kivshar, Opt. Commun. **285**(5), 821–824 (2012).
[17]D. Dregely, R. Taubert, J. Dorfmuller, R. Vogelgesang, K. Kern, and H. Giessen, Nat. Commun. **2**(4), 267 (2011).
[18]E. W. McFarland and J. Tang, Nature **421**, 616 (2003).
[19]L. Novotny, Phys. Rev. Lett. **98**(26), 266802 (2007).
[20]Y. Gu, J. P. Romankiewicz, J. K. David, J. L. Lensch, and L. J. Lauhon, Nano Lett. **6**(5), 948–952 (2006).
[21]J. Burm, K. I. Litvin, D. W. Woodard, W. J. Schaff, P. Mandeville, M. A. Jaspan, M. M. Gitin, and L. F. Eastman, IEEE J. Quantum Electron. **31**(8), 1504–1509 (1995).
[22]W. L. Barnes, A. Dereux, and T. W. Ebbesen, Nature **424**, 824 (2003).
[23]A. V. Zayats, I. I. Smolyaninov, and A. A. Maradudin, Phys. Rep. **408**(3–4), 131–314 (2005).